Received: 2 August 2022 | Revised: 17 November 2022 | Accepted: 21 November 2022

DOI: 10.1002/app.53483

RESEARCH ARTICLE

Applied Polymer SCIENCE WILEY

Mechanical and radiation shielding properties of SWCNT reinforced polymer/glass fiber fabric-based nanocomposite containing different filler materials: A comparative study

Ali Murat Sürücü[1] | **Serkan Subaşı**[2] | **Aamar Danish**[3] | **Osman Gencel**[4] | **Azime Subaşı**[5] | **Togay Ozbakkaloglu**[3]

[1]Composite Materials Technology Division, Düzce University, Düzce, Turkey

[2]Engineering Faculty, Civil Engineering Department, Düzce University, Düzce, Turkey

[3]Ingram School of Engineering, Texas State University, San Marcos, Texas, USA

[4]Engineering Faculty, Civil Engineering Department, Bartin University, Bartin, Turkey

[5]Gümüşova Vocational School, Metallurgy Department, Düzce University, Düzce, Turkey

Correspondence
Togay Ozbakkaloglu, Ingram School of Engineering, Texas State University, San Marcos, TX-78666, USA.
Email: togay.oz@txstate.edu

Abstract

In this study, polymer/glass fiber fabric-based nanocomposite plates were fabricated with 0.01%–0.1% single-walled carbon nanotubes (SWCNTs) and filler materials (barite, magnetite, and colemanite) using a hand layup process. Mechanical properties (e.g., tensile strength, flexural strength, and Charpy impact strength), thermal conductivity, and radiation shielding properties (e.g., gamma radiation and neutron radiation) of the specimens were determined. The results revealed that the specimens containing barite and magnetite managed to exhibit adequate mechanical properties (especially Charpy impact strength). Among different filler materials used, barite-filled specimens outperformed colemanite and magnetite-filled specimens in terms of mechanical properties. The mechanical performance of filler-modified specimens can be further enhanced by adopting efficient dispersion techniques to disperse filler material and SWCNTs throughout the composite plates. The thermal conductivity of barite, magnetite, and colemanite-filled specimens (with/without SWCNTs) increased by 30.56%–60% as compared to specimens only containing SWCNTs and neat polymer, which avoids the accumulation of heat required for radiation shielding applications. Similar to thermal conductivity, specimens containing filler materials (with and without SWCNTs) provided higher gamma and neutron radiation shielding properties as compared to neat polymer- and SWCNT-modified specimens. In the case of gamma and neutron radiation shielding, barite- and colemanite-filled specimens provided better results, respectively.

KEYWORDS

barite, colemanite, magnetite, mechanical properties, nanocomposite, radiation shielding, SWCNTs

1 | INTRODUCTION

The utilization of high-energy radiation (like gamma rays (γ-rays) and neutron rays (N-rays)) is rapidly increasing in various sectors such as agriculture (to produce and improve new genetic lines of root and tuber crops, cereals, and oil seed crops),[1,2] biological studies (learn about the methods to inactivate viruses[3] and repair human lymphocytes[4]), medical diagnostics (medical imaging[5] and radiopharmaceuticals[6]), and space exploration (understand the laws of physics in the hostile environments of distant universes,[7,8] and detect the concentration of different elements on other planetary objects).[9,10,11] However, being highly powerful and penetrating in nature, unnecessary exposure to the mentioned radiation may pose a detrimental impact on the environment, human health, and other materials.[12,13] In particular, in the case of human health, this can cause cancer, cell mutation, component failure, organ damage, radiation sickness, and other detrimental effects.[14] Hence, protection against the unfavorable effects of inadvertent radiation on the environment and human health is essential.

For the past decade, researchers have been investigating affordable and easy-to-produce polymer-based composites with radiation shielding capabilities and improved mechanical properties.[15–18] Some recent experimental studies evaluated various composite materials as potential radiation shielding composites, for example, epoxy/lead composites,[19–21] epoxy/gadolinium (III) oxide composites,[22] silicon resin/additives composites,[23] epoxy/tungsten composites,[24] and nanoconcrete composites.[25–27] Traditional fiber-reinforced polymer composites (FRPCs) are a broad category of materials that have been considerably researched for various applications in different industries like automotive, aviation, deep-sea/space exploration, and energy harvesting. This can be credited to their low weight, excellent mechanical properties, improved durability properties, high fatigue strength, and outstanding surface finishes.[28] In addition, FRPCs have the potential to be used as advanced high-strength multifunctional materials in high-risk industries for various applications like radiation shielding.[29] In FRPCs, the polymer constituent is flexible and can alter its structural and mechanical properties[29] because when utilizing FRPC for radiation shielding, specific changes in their structural and mechanical characteristics become an important parameter in evaluating their suitability. One of the types of FRPC is glass fiber-reinforced polymeric composite (GFRPC), which has been used in a variety of industrial applications due to its high stiffness, high strength, excellent resistance against impact loading, and high durability.[30] The excellent properties of GFRPC are mainly due to the glass fiber having high chemical stability, high mechanical strength, and moisture insulation.[31]

Recently, research institutes and scientific groups have reported that various polymer matrices can be used for radiation shielding applications, such as boron/polyethylene modified polymer composites,[10] lead monoxide incorporated polymer composites,[32] light-weight bismuth nanoparticles based polymer composites,[33] lead (II) chloride modified polymer composites,[34] boron and wolfram carbide filled polymer composites,[35] lead modified polymer composites,[36] nanosized lead FRPC,[37] silicon polymer composites,[38] lead oxide polymeric nanocomposites,[39] niobium incorporated polymer composite,[40] lead (II) added polymer composites.[41]

Although base materials used to prepare polymer composites possess necessary electrical properties and are excellent insulators; however, this property can be enhanced by incorporating micro/nano-sized filler materials as they impart special properties to the resins, reduce cost, and decrease thermal strains due to the variations in the coefficient of thermal expansion.[42,43] However, increasing the amount of filler materials may also increase the cost of composites, especially in resource-deficient countries. The carbon nanotubes (CNTs) have an exceptional combination of stiffness and mechanical properties, high aspect ratio, low density, and negative thermal expansion coefficient,[44–46] which makes them perfect multifunctional materials to be added to FRPC. It is noteworthy that similar shielding levels of filler-incorporated composites for radiation shielding can be achieved by the incorporation of a relatively lower quantity of nanosized filler (like CNTs [single/multi-walled]).[47] Considering the benefits of incorporating micro/nanosized, it is imperative to investigate the optimal mix proportions of composite materials containing both microsized and nanosized fillers to maximize radiation-shielding properties without increasing cost. This can be achieved by incorporating low-cost, abundantly available, easy-to-process micro/nanosized filler materials.

The term barite is used for a mineral group including anglesite, barium sulfate, celestite, and anhydrite minerals. Barite is abundantly available worldwide, particularly in China, Germany, India, Mexico, Pakistan, Turkey, and the U.S., accounting for more than 80% of barite exports worldwide.[48] The specific gravity of barite is very high, making it suitable for industrial, medical, and manufacturing sectors. Colemanite is similar to diamond in terms of hardness and appearance, and it is abundantly available worldwide, especially in Turkey, the U.S., and Russia. Out of 200 different boron

materials, colemanite is abundantly available in more than 70% of all boron deposits with Turkey having the largest deposits in the world.[49] Colemanite is used in the manufacturing of glass, cutting-edge ceramics,[50] attenuation of γ-rays,[51] and neutron radiation.[52] Magnetite is one of the most abundantly available natural materials as iron oxide (Fe_3O_4). Magnetite can also be artificially produced in nanometric size using chemical synthesis techniques such as the precipitation method and sol–gel method.[53] Nowadays, a wide range of applications of magnetite can be witnessed in pharmaceuticals,[54] cancer therapy,[55] radiation shielding,[56,57] and magnetic resonance imaging.[58]

The investigation of mechanical behavior, thermal conductivity, and radiation shielding properties of polyester/glass fiber fabric-based nanocomposites containing 0.01%–0.1% of SWCNTs and micronized filler materials (such as colemanite, barite, and magnetite) is the novelty of this experimental study. The emphasis is given to the comparison and optimization of mechanical properties (i.e., tensile strength, flexural strength, and impact strength), thermal conductivity, and radiation shielding properties (i.e., γ-radiation and N-radiation) of polymer-based nanocomposite with different proportions of SWCNT and the mentioned filler materials.

2 | MATERIALS AND METHODS

2.1 | Materials

2.1.1 | Polymer resin

Terephthalic unsaturated polyester resin with high mechanical and fiber wetting ability was acquired from the Turquoise polyester company for this study. The liquid properties of the resin are given in Table S1, and the pure mechanical properties are given in Table S2.

2.1.2 | Glass fiber fabric

WR 125–500 model E-type bidirectional woven GF was obtained from Şişecam for this study (see Figure S1). The technical specifications of the GF used are given in Table S3.

2.1.3 | SWCNTs

OCSIAL Tuball Matrix-204 model SWCNTs were used as the nano-reinforcement phase in this study. The secondary electron microscope (SEM) image of SWCNT with different magnifications is shown in Figure S2.

2.1.4 | Barite, colemanite, and magnetite

In this study, barite, colemanite, and magnetite were used as filling materials obtained from Aromel Chemistry Inc., Eti Mining, Balikesir, and Erdemir Mining Divrigi, respectively (see Figure S3). The technical properties of barite, colemanite, and magnetite are given in Table S4. The grade size analysis of barite, colemanite, and magnetite is shown in Figure 1. The filling materials obtained after passing them through a 300-mesh sieve were used in this study.

2.2 | Preparation of nanocomposites

The hand layup method was used to prepare nanocomposite plates with the required specifications. In this method, the matrix material containing the initiator, accelerator, and reinforcement material was placed in the mold in layers, and a roller/brush was used to disperse the matrix material on the reinforcement material. The following steps were adopted to successfully prepare nanocomposite plates using the hand layup technique:

1. The GF was cut in the dimensions of 350 × 450 cm^2 (see Figure S4). For each composite plate, five layers of GF were prepared. The total weight of five layers of GF used for each composite plate is 480 g.
2. To avoid early or late curing problems during the preparation of composite plates, initiator and accelerator ratios are determined for each filler material by measuring the gelling times of 100 g of trail castings. The gelling times of trail castings were determined at room temperature (25°C) as per the specifications mentioned in ISO 2535:2001.[59] Cobalt octoate and MEK-P were used as accelerator and initiator in the trail castings, respectively, in the following ratios: (0.1%, 0.2%, 0.3%, 0.4%, 0.5%, 1%, and 1.5%) and (1%, 1.5%, 2%). The polyester resin, filler material (barite/colemanite/magnetite), and accelerator were mixed for 2–3 min using an ISOLAB magnetic stirrer, followed by 1 min mixing by adding the initiator. The gelation times for different mixes prepared were measured by pouring them into Petri dishes. Some of the trial castings in the Petri dishes are shown in Figure 2. The optimal gelation times and accelerator-to-initiator ratios for different specimens are given in Table 1.

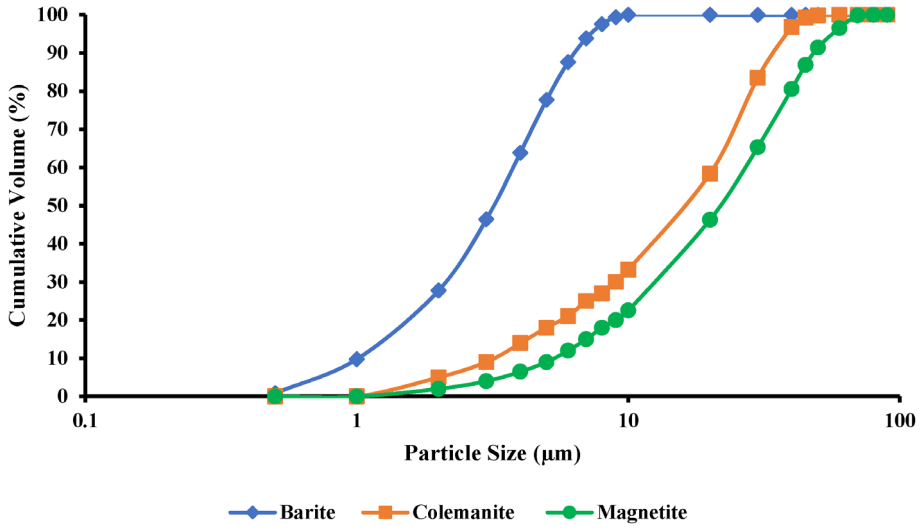

FIGURE 1 Particle size analysis of barite, colemanite, and magnetite. [Color figure can be viewed at wileyonlinelibrary.com]

FIGURE 2 Trial castings of raw resin, resin + barite, resin + magnetite, and resin + colemanite (from left to right) [Color figure can be viewed at wileyonlinelibrary.com]

TABLE 1 Gelation times and accelerator-to-initiator ratios of different specimens prepared

Sample type	Accelerator to initiator	Gelation time (min)
Resin + barite	1.5:1	38
Resin + magnetite	0.5:1	32
Resin + colemanite	0.1:1	26
Raw resin	0.2:1	43

TABLE 2 The amount of SWCNTs taken from the tri-ethylene glycol di-methacrylate solution according to the usage rate

Desired incorporation of SWCNTs (%)	Amount supplemented by ratio* (g)	Amount of SWCNTs taken from 10% solution (g)
0.01 SWCNT	0.05	0.5
0.05 SWCNT	0.25	2.5
01 SWCNT	0.5	5

[a]The specified SWCNT ratios are calculated for 500 g resin.

3. The dispersion of SWCNTs was carried out using the suspension method. The SWCNTs used in this study were in the form of 10% tri-ethylene glycol di-methacrylate solution. Thus, 0.01%–0.1% SWCNTs were calculated from the mentioned solution as given in Table 2. The calculated amount of SWCNTs was mixed with 500 g of raw resin in a mixer at a rotational speed of 2500 rpm for 20 min (see Figure S5a) followed by degassing using a Bandelin Sonorex ultrasonic bath to maintain the temperature and remove the air bubbles formed after the process (see Figure S5b). For the specimens containing filler

TABLE 3 Mix proportions and nomenclature of specimens

Specimen	Glass fiber fabric	Resin (wt%)	SWCNT by resin weight (wt%)	Barite (wt%)	Magnetite (wt%)	Colemanite (wt%)
REF	5 layers	50	—	—	—	—
SC-1	5 layers	49.99	0.01	—	—	—
SC-2	5 layers	49.95	0.05	—	—	—
SC-3	5 layers	49.9	0.1	—	—	—
BREF	5 layers	25	—	50	—	—
BSC-1	5 layers	24.99	0.01	50	—	—
BSC-2	5 layers	24.95	0.05	50	—	—
BSC-3	5 layers	24.9	0.01	50	—	—
MREF	5 layers	25	—	—	50	—
MSC-1	5 layers	24.99	0.01	—	50	—
MSC-2	5 layers	24.95	0.05	—	50	—
MSC-3	5 layers	24.9	0.01	—	50	—
CREF	5 layers	25	—	—	—	50
CSC-1	5 layers	24.99	0.01	—	—	50
CSC-2	5 layers	24.95	0.05	—	—	50

material, filler material (barite/colemanite/magnetite) was mixed with SWCNT dispersion resin for another 5 min in another mechanical mixer after degassing. The resin-to-filler ratio used for this study is 1:2.

For the preparation of composite plates via the hand layup method, the wooden laths of $10 \times 20\ mm^2$ were glued together to form a $400 \times 500\ mm^2$ rectangular frame, and the molds were prepared by gluing the frames to the glass counter. Then, the upper mold glass was prepared beforehand by cutting to $300 \times 400\ mm^2$ dimensions, and the glass counter, Frekote 770-NC mold release agent was applied 3 times with a 15-min drying time. After the mold release application, since there were five layers of GF on each plate, the resin was weighed for six layers and divided into six parts and was applied to the matrix material equally to each layer. After the matrix material was poured and spread for the first layer, the GF layer was placed, and the matrix material was poured on it again so that the GF was completely wet with the help of an aluminum fiber-crushing roller. This application was repeated until the end of the process, and after the top layer was laid, the upper mold glass was closed in such a way that the surface on which the release agent was applied was placed on the material, and 50 kg weight was placed on it for curing at room temperature as shown in Figure S6a. Some of the composite plate plates prepared by this process are displayed in Figure S6b.

2.3 | Preparation of test specimens

The test specimens were obtained by cutting the composite plates prepared according to the standards listed in Table S5. The cutting process was carried out in a vacuum computer numerical control (CNC) router machine, which is a fully automatic machine and provides precise control of the processing bench with computer support. Some of the test specimens prepared for this study are shown in Figure S7.

For this study, 15 specimens were initially planned, but owing to the higher viscosity and increase in temperature of SWCNT reinformed composites containing colemanite, flexural strength, tensile strength, and impact strength tests were only conducted on composites containing SWCNT and barite/magnetite. The mix proportions and nomenclature of specimens prepared for this study are given in Table 3.

2.4 | Methods

2.4.1 | Viscosity

Before starting the production of composite plates, viscosity measurements of all resins prepared were made by following ISO 2555[60] with Brookfield Method VISCO-TECH VR 3000 dynamic viscosity tester.

2.4.2 | Tensile strength, flexural strength, and charpy impact strength

The tensile strength test was carried out as per ISO 527-4[61] at a loading speed of 1 mm/min. The length and width of all specimens subjected to the tensile test were measured with the help of a digital caliper.

The flexural strength test of the composite samples was carried out as per ASTM D7264-21.[62] For this test, the distance between the supports was 128 mm, and the loading speed was adjusted to 1 mm/min.

The Charpy impact strength tests of the composite samples were carried out as per ISO 179.[63] The height, length, and width values of all samples were measured with a digital caliper.

2.4.3 | Thermal conductivity, γ-radiation shielding, and N-radiation shielding

Thermal conductivity was measured with a TCi-Thermal Conductivity Analyzer on $20 \times 20\ mm^2$ specimens. The γ-attenuation performance of the composite plates was carried out at the Turkish Energy, Nuclear, and Mining Research Institute with the help of the experimental setup shown in Figure S8. The γ-radiation shielding potential of composite specimens can be determined via linear attenuation coefficient (LAC) and mass attenuation coefficient (MAC). The value of LAC was evaluated using ^{60}Co as a γ-ray energy source. Technical information about the measurement system is shown in Table S6. Generally, the γ-rays interact with the materials either by scattering away or absorption, which can be expressed as per Equation (1). The MAC was measured by diving LAC by the density of the specimen as per Equation (2). Thickness of the material required to decrease the initial radiation intensity to 50% after passing through the material is known as the half-value layer (HVL) and can be determined by Equation (3). The thickness of the material required to decrease the initial radiation intensity to 10% after passing through the material is known as the tenth-value layer (TVL) and can be determined by Equation (4).

$$I = I_o e^{-\mu x} \tag{1}$$

$$MAC = \frac{LAC}{Density} \tag{2}$$

$$HVL = \frac{0.693}{\mu} \tag{3}$$

$$TVL = \frac{2.303}{\mu} \tag{4}$$

Where, I, I_o, x, and μ is intensity of the passing photon beam, intensity of the incident photon beam, thickness of specimens, and LAC, respectively.

The Turkish Energy, Nuclear, and Mining Research Institute's laboratory tested the N-attenuation performance of composite plates. Table S7 shows the measurement system's technical data. Because there is always some N-radiation around the howitzer, background counts of N-dose in the medium were conducted before starting specimen irradiation. Then, with a total of 225 counts, each specimen with three different thicknesses was analyzed against N-radiation. The experimental setup to determine the performance of N-rays attenuation by composite plates is shown in Figure S9.

3 | RESULTS AND DISCUSSION

3.1 | Viscosity

The viscosity of the matrix with varying quantities of SWCNT and filler materials (barite/magnetite/colemanite) is shown in Figure 3. As can be observed from the figure, the viscosity values of specimens vary in a wide range, with SC-1 and CREF experiencing the lowest and highest viscosity, respectively. Though the incorporation of filler materials and SWCNTs increased the viscosity of the specimens, the filler materials had a more negative impact on the viscosity as compared to the addition of SWCNTs, which is contrary to the fact that the incorporation of material with a higher specific area (or smaller particle size) decreases viscosity. For example, the SC-1 experienced 765%, 1869%, and 4592% lower viscosity as compared to BREF, MREF, and CREF, respectively. The high viscosity of specimens containing filler materials as compared to SWCNTs can be attributed to a higher percentage of filler materials as compared to the SWCNTs. The addition of filler materials may lead to agglomeration due to the interaction between the filler material and polymer matrix, leading to increased viscosity. Moreover, the higher viscosity of composites containing filler materials can also be ascribed to the transition from liquid-like to solid-like viscoelastic response.[64,65] On the other hand, the lower viscosity of specimens containing SWCNTs can be credited to the shearing thinning property of SWCNT owing to its unidimensional chain structure. To some extent, SWCNTs might have been oriented at a high shearing rate, leading to a decrease in viscosity.[66] Moreover, the addition of SWCNT may increase the disentanglement of polymer chains because SWCNTs act as streamliners for the flow of polymer chains, which is consistent with the previous studies on multiwalled CNTs-

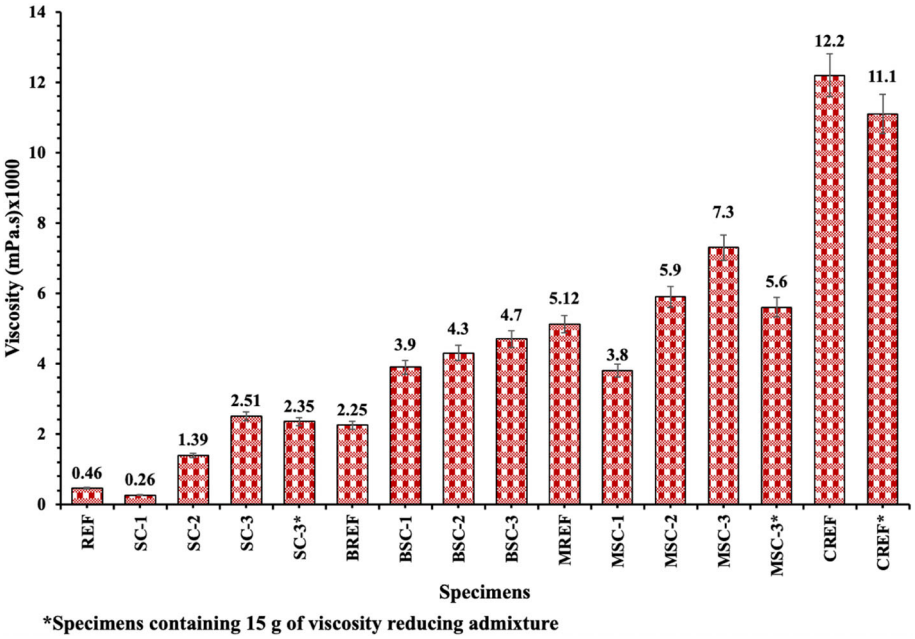

FIGURE 3 Viscosity of specimens with different filler materials and amount of SWCNTs [Color figure can be viewed at wileyonlinelibrary.com]

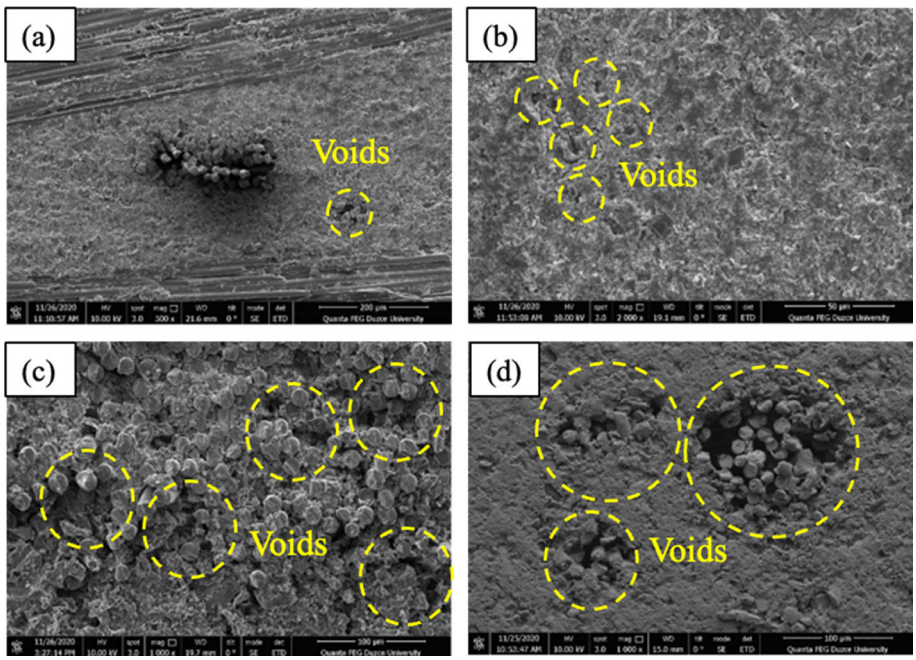

FIGURE 4 SEM images of (a) REF, (b) BSC-2, (c) MSC-3, (d) CREF [Color figure can be viewed at wileyonlinelibrary.com]

polypropylene composite sheets[67] and multiwalled CNTs-polypropylene composite.[68]

The SWCNT-reinforced polymer resin containing different filler materials showcased a further increase in viscosity. SWCNT incorporation increased specimen viscosity, which can be attributed to supramolecular interaction between SWCNTs due to van der Waals forces, making them difficult to disperse in the polymer matrix, resulting in the agglomeration and increased viscosity.[69,70] The SWCNT-reinforced polymer resin containing barite has the lowest viscosity as compared to the specimens containing magnetite and colemanite. However, the addition of 0.01% SWCNTs decreased the viscosity of a specimen containing 50% magnetite, which was not observed in the case of barite or colemanite-filled composites. In the case of composites filled with colemanite, viscosity reaches 12,200 mPa.s and the incorporation of SWCNTs in colemanite-filled specimens further increases the viscosity, making it difficult to measure. This indicates that the incorporation of colemanite leads to the transition of polymer resin from viscous liquid to solid-like behavior. In other words, the rheology of polymer resin containing colemanite experiences a transition from a rheological state (where viscosity alters

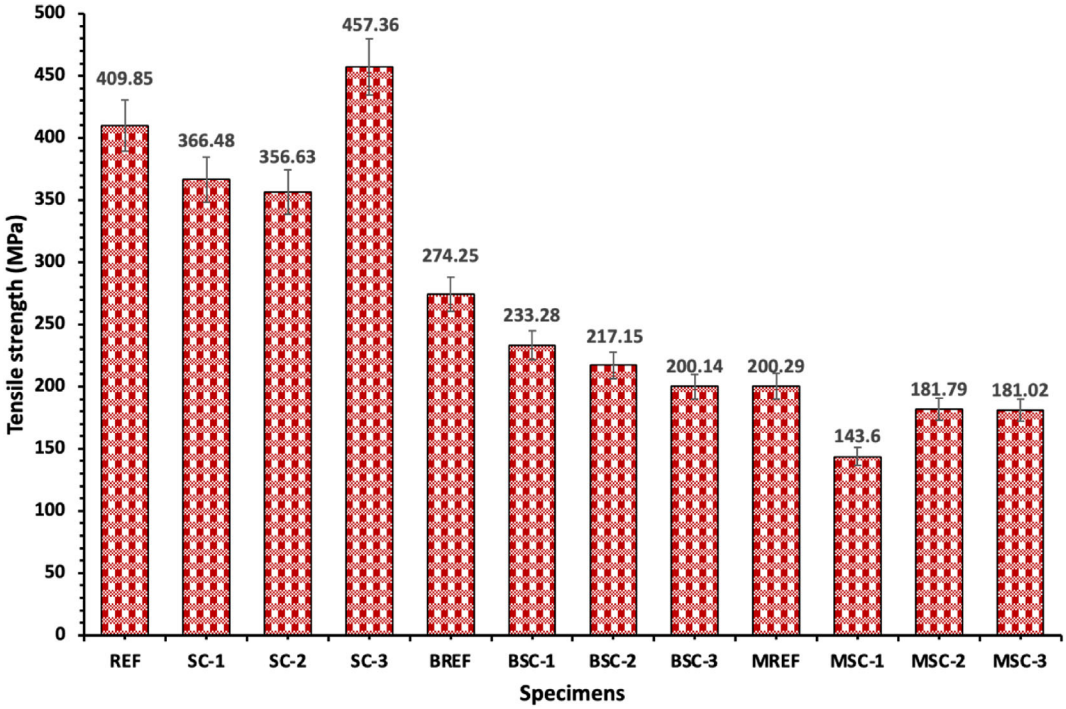

FIGURE 5 Tensile strength of specimens with different filler materials and amount of SWCNTs [Color figure can be viewed at wileyonlinelibrary.com]

considerably with increasing filler quantity) to solid-like behavior (where viscosity is insensitive to increasing filler quantity), which is known as the rheological percolation threshold.[71,72] To decrease the viscosity, SWCNT-reinforced polymer resin containing filler materials was modified with a viscosity-reducing admixture followed by mixing for 4–5 min. However, it did not help significantly in reducing viscosity, particularly in the case of specimens containing colemanite. Therefore, the fabrication of colemanite-incorporated composite plates to prepare test specimens and investigate their performance was not possible.

SEM images also give an idea of the viscosity of specimens prepared as shown in Figure 4a–d. Figure 4a shows the SEM image of REF with no or negligible voids, which indicates that neat polymer resin effectively wets the surface of GF. On the other hand, specimens containing barite, magnetite, and colemanite have small, medium, and large sized voids (see Figure 4b–d), respectively. In other words, the most successful homogenous distribution and matrix-reinforced interface can be observed in REF and specimens containing barite, which is consistent with the previous study on barite-filled acrylonitrile butadiene styrene composites.[73] Therefore, based on the dispersion homogeneity, specimens can be ordered as net polymer > barite-filled specimens > magnetite-filled specimens > colemanite-filled specimens along with a few exceptions, particularly for the specimens containing both SWCNT and filler materials. This also impacts the mechanical and radiation shielding properties of specimens as discussed in the later sections.

3.2 | Mechanical properties

The tensile strength of specimens with different filler materials and amount of SWCNTs is shown in Figure 5. As per the figure, specimens containing neat polymer and SWCNT exhibited higher strength as compared to the specimens containing filler materials. The addition of SWCNT showed variable impacts on the composite with and without filler materials. For example, the incorporation of 0.01%–0.05% SWCNTs (SC-1 and SC-2) decreased the tensile strength of the specimen as compared to REF, while increasing the incorporation of SWCNT to 0.1% increased the tensile strength by 11.59% as compared to REF. The increase in the tensile strength of SWCNT-reinforced specimens can be credited to the alteration of chemical and mechanical properties of polymer resin via SWCNT, leading to the strengthening of interfacial properties of GF, which is aligned with the results reported by previous studies.[31,74] Moreover, the accumulation of SWCNT in the polymer resin acts as a rigid body, prevents crack growth in the direct path, and prolongs the crack path, leading to increased tensile strength of SWCNT-reinforced polymer composites.[31] Previous studies conducted on SWCNT/polymer composites[75–78] revealed

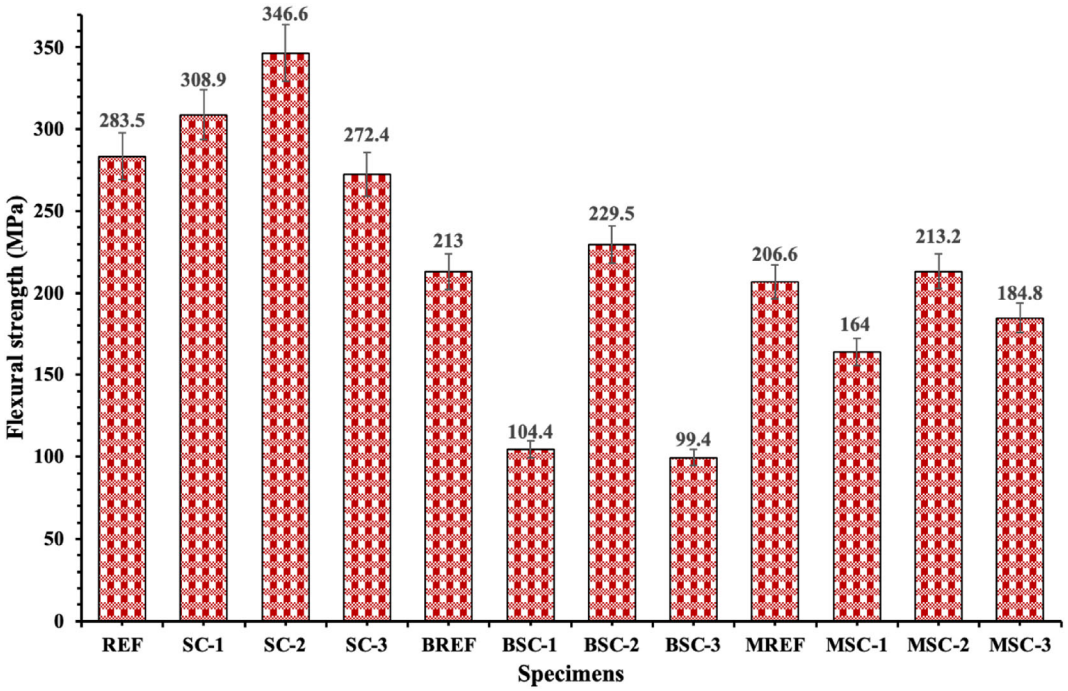

FIGURE 6 Flexural strength of specimens with different filler materials and amount of SWCNTs [Color figure can be viewed at wileyonlinelibrary.com]

that three main factors affect the reinforcement of SWCNT/polymer composites: (1) dispersion of SWCNTs in the polymer matrix; (2) strong interfacial bonding between SWCNTs and polymer; and (3) appropriate alignment of SWCNTs in the polymer matrix. For the study, the most suitable attribution for the increase in tensile strength of SWCNT/polymer composites is the effective dispersion of SWCNTs in the polymer matrix that negates any possibility for the formation of agglomerates and consequential voids.

On the other hand, SWCNT did not help in increasing the tensile strength of specimens containing filler materials. For example, BREF, BSC-1, BSC-2, and BSC-3 exhibited 33.08%, 43.08%, 47.02%, and 51.17% lower tensile strength as compared to REF, respectively. Similarly, MREF, MSC-1, MSC-2, and MSC-3 experienced 51.13%, 64.96%, 55.64%, and 55.83% lower tensile strength as compared to REF, respectively. The decrease in tensile strength of specimens containing filler materials can be attributed to poor dispersion of barite and magnetite in the polymer matrix, leading to agglomeration and voids as revealed by SEM images shown in Figure 4. Moreover, the tensile strength of barite-filled specimens superseded the specimens containing magnetite, which is justified by the greater number of voids in the magnetite-filled specimens (see Figure 4c). The addition of SWCNTs in the specimens containing filler materials decreased the tensile strength because SWCNTs aggravated the process of agglomeration, leading to the weak interaction between SWCNTs and the polymer matrix. Previously published studies[73,79] on nanomaterial reinforced polymer composites containing filler materials reported that incorporation of 5% filler material can improve the tensile strength while further increase in filler material leads to agglomeration. As in this study, the usability of 50% filler material makes it an obvious reduction in the tensile strength.

The flexural strength of specimens with different filler materials and amount of SWCNTs is shown in Figure 6. As shown in the figure, SC-2 experienced the highest flexural strength while BSC-2 exhibited the lowest flexural strength. The flexural strength of SC-1 and SC-2 showed 8.95% and 22.25% higher flexural strength as compared to REF, respectively. On the other hand, SC-3 exhibited a 4.07% lower flexural strength as compared to REF. The higher flexural strength of specimens containing 0.01% and 0.05% SWCNTs can be ascribed to the dispersion of SWCNTs that restrict the movement of polymer chains under loadings. The high modulus, aspect ratio, and strength of SWCNTs and good interfacial adhesion between the matrix and SWCNTs also improved the flexural strength of SWCNT-modified specimens,[80] which is consistent with the previous studies.[76,81–83] The lower strength of REF is due to the greater speed of crack motion, when the poor interfacial bond between the two phases of the GF and matrix, the cracks can easily

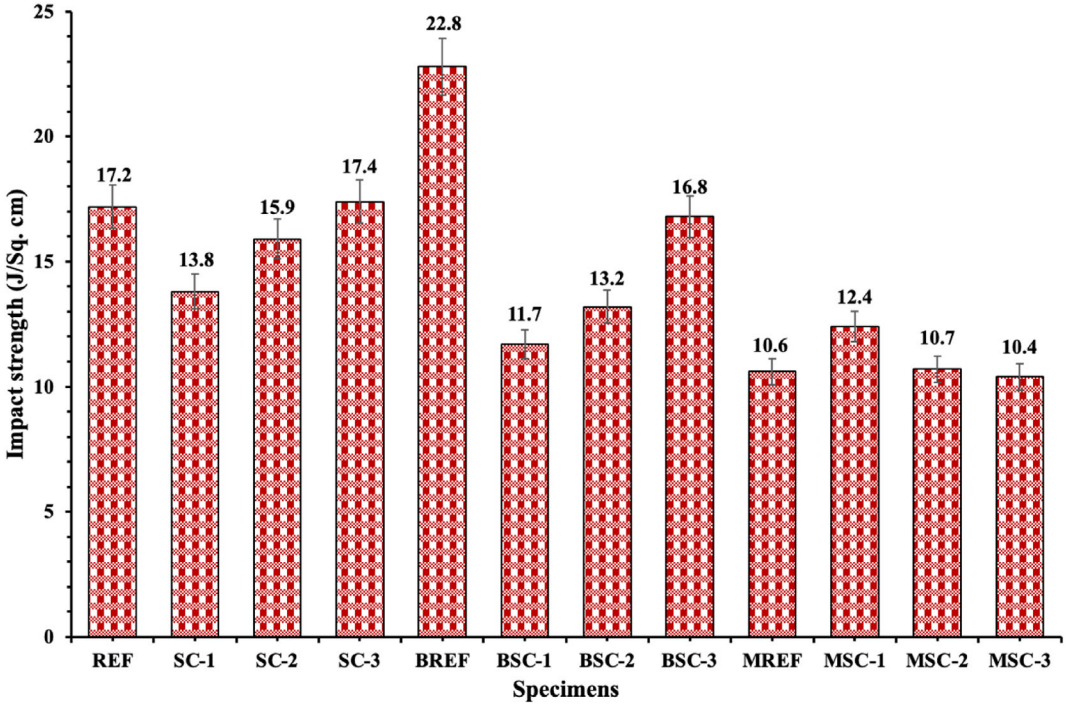

FIGURE 7 Charpy impact strength of specimens with different filler materials and amount of SWCNTs [Color figure can be viewed at wileyonlinelibrary.com]

grow in the respective direction. Conversely, the addition of SWCNTs can considerably contribute to the strength of specimen joints that may limit the growth of cracks. As a result, with the occurrence of such a phenomenon, much more energy is required to move the crack, leading to an increase in the amount of energy absorption in the specimens referred to as the crack bridging effect.[84–86]

The specimens containing filler materials exhibited reduced strength as compared to neat polymer composite and SWCNT-modified specimens. For example, BREF, BSC-1, BSC-2, and BSE-3 experienced 24.87%, 63.17%, 9.04%, and 64.93% lower flexural strength as compared to REF, respectively. Similarly, the flexural strength of MREF, MSC-1, MSC-2, and MSC-3 was reduced by 27.12%, 42.15%, 24.79%, and 34.81%, respectively, as compared to REF. The negative influence of filler materials on the flexural strength of composite specimens is in accordance with a previous study.[87] However, in the previous studies, the decrease in the flexural strength of polymer composites containing filler materials was lower as compared to this study, which can be attributed to different specimen thicknesses, incorporation levels of filler materials, dispersion techniques used to disperse nanomaterials, and so forth. Compared to the specimens containing SWCNTs (without filler materials), the percentage decrease in the flexural strength of specimens containing barite and magnetite was more pronounced. The decrease in flexural strength of specimens containing filler materials can be attributed to high incorporation levels, which generally results in filler agglomeration, that is, the filler particles arrange themselves in very close proximity to one another making particle size significantly larger, leading to an increase in flaw size. However, it is debatable whether the decrease in flexural strength is due to this phenomenon.[88] The decrease in flexural strength of filler-incorporated specimens was slightly increased by adding 0.05% SWCNTs, which can be attributed to the elasticity and flexibility provided by SWCNTs to the specimen. It is interesting to note that the flexural strength of different magnetite-filled specimens experienced smooth increasing/decreasing variation while the variation in flexural strength of barite-filled specimens was abrupt. For example, the flexural strength of magnetite-filled and barite-filled specimens ranged between 164–213.2 MPa and 99.4–229.5 MPa, respectively. Moreover, the flexural strength of BREF and BSC-2 is 3.09% and 7.64% higher than that of MREF and MSC-2, respectively. On the other hand, the flexural strength of BSC-1 and BSC-3 is 36.34% and 45.98% lower as compared to MSC-1 and MSC-3, respectively.

Figure 7 shows the Charpy impact strength of specimens with different filler materials and amount of SWCNTs. As per the figure, BREF showed the highest impact strength, while the minimum impact strength

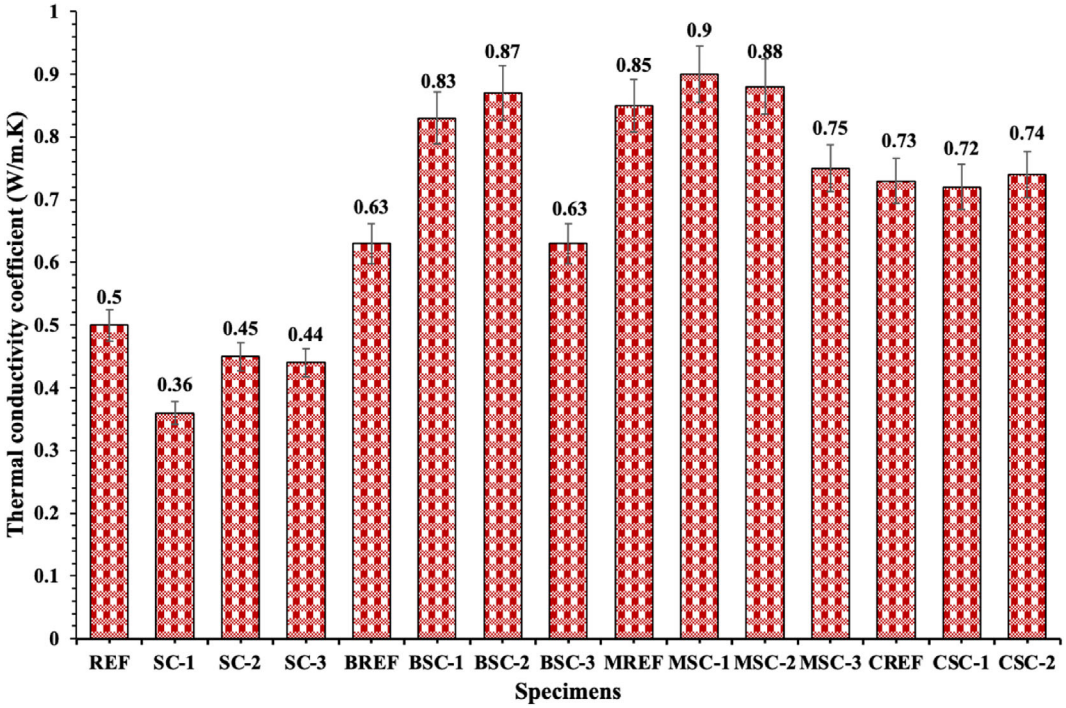

FIGURE 8 TCC of specimens with different filler materials and amount of SWCNTs [Color figure can be viewed at wileyonlinelibrary.com]

was observed for MSC-3. Unlike tensile strength and flexural strength, SWCNTs do not provide a significant positive impact on the impact strength of specimens. For instance, the impact strength of SC-1 and SC-2 is 19.77% and 7.56% lower than REF, while SC-3 experienced slightly higher (1.16%) impact strength as compared to REF. In the previous studies, the higher impact strength of polymer composite specimens was achieved by incorporating CNTs greater than 0.1%, which justifies the lower impact strength of SC-1 and SC-2 and the slightly higher impact strength of SC-3 as compared to REF.

The barite and magnetite-filled specimens with or without SWCNTs show a variable effect on the impact strength. For example, the impact strength of BREF is 32.56%, 65.22%, 43.4%, and 9.43% higher than REF, SC-1, SC-2, and SC-3, respectively. The increase in impact strength of BREF can be credited to considerable interfacial adhesion between barite and polymer matrix, which effectively transfers stress from the polymer matrix to the filling material. This observation is aligned with the previous studies on barite-filled polymer composites.[73,89] For example, Huang et al.[89] revealed that the incorporation of 10%, 20%, 30%, and 40% barite reduced the impact strength of polymer composite by 43.47%, 11.33%, 9.48%, and −0.98%, which indicates that the incorporation of 10% barite significantly decreased the impact strength while increasing amounts of barite showed an increasing trend and finally superseded the control mix at 40% barite content. Figure 7 shows that the incorporation of SWCNTs led to a sudden decrease in the impact strength as compared to BREF but increasing the percentage of SWCNTs in BSC-2 and BSC-3 resulted in increasing impact strength, which is similar to the trend observed in SC-1, SC-2, and SC-3. On the other hand, the addition of magnetite significantly reduced the impact strength of specimens; for example, the impact strength of MREF is 38.37% lower than REF. This can be credited to the formation of stress-failure zones on the interface between magnetite and polymer matrix. However, the incorporation of SWCNTs in magnetite-filled specimens exhibited different results as compared to the addition of SWCNTs in neat polymer and barite-filled specimens. For example, MSC-1 experienced 16.98%, 15.88%, and 19.23% higher impact strength as compared to MREF, MSC-2, and MSC-3, respectively, which can be credited to the bridging effect provided by SWCNTs while further increase in SWCNTs led to agglomeration.

3.3 | Thermal conductivity

Figure 8 shows the thermal conductivity coefficient (TCC) of specimens with different filler materials (barite, colemanite, and magnetite) and amount of SWCNTs. The TCC is an important parameter for the composites to be used for radiation shielding applications because it helps release

heat generated during the nuclear reactions.[51] The TCC of REF is 0.5 W/m.K, which is consistent with previous studies reporting that the TCC of neat polymer is between 0.2 and 0.5 W/m.K. The low TCC of REF can be attributed to the scattering of inherent phonons between the polymer chain ends and impurities, making it challenging to expedite heat transfer.[90,91] The addition of SWCNTs did not have a positive influence on the TCC of specimens, for example, the TCC of SC-1, SC-2, and SC-3 is 28.1%, 10.03%, and 12% lower than the REF, respectively. As per previous studies, this can be credited to high contact resistance between CNTs and high interfacial resistance between polymer resin and CNTs. The transport of phonons in CNTs is restricted by contact resistance, while the interfacial resistance detrimentally impacts the transfer of phonons between polymer resin and CNTs.[92,93] For the mentioned reasons, SC-1 experienced a significant drop in TCC, whereas increasing the percentage incorporation of SWCNTs to 0.05% improved the TCC of SC-2 by 25% as compared to SC-1. However, further increasing the amount of SWCNTs to 0.1% reduced TCC by 2.22% compared to SC-3. This indicates that different factors affect the TCC of CNT-reinforced polymer composites, including the length of CNTs, dispersion of CNTs, percentage incorporation of CNTs, type of polymer, the addition of micro-sized filler, and so forth. For example, as compared to this study, previous studies reporting higher TCC of SWCNT-reinforced polymer composites as compared to neat resin can either be attributed to the utilization of better dispersion techniques or a higher incorporation percentage of SWCNTs.[94,95] Nonetheless, even at a higher incorporation percentage of SWCNTs, the TCC reported by some of the previous studies (e.g., reference 96) is low as compared to this study, which can be attributed to the interdependence of the mentioned parameters on the TCC of CNT-polymer composites.

Figure 8 shows that the addition of filler materials has a beneficial effect on the TCC of specimens. For example, BREF, MREF, and CREF increased TCC by 26.01%, 70.03%, and 46.02% as compared to REF, respectively. The increase in TCC of filler-incorporated polymer composites can be ascribed to the formation of bridges among filler particles within a polymer matrix referred to as conductive networks. The development of random networks or bridges from filler particles aids the transfer of phonons or electrons, leading to high thermal conductivity.[97] By comparing the effectiveness of filler materials in increasing the TCC of polymer composites, MREF has a higher TCC as compared to BREF and CREF, which can be attributed to the larger particle size of magnetite. Based on the particle size (or surface area) of filler materials used in this study (see Table S4), the TCC of specimens containing filler materials (without SWCNTs) can be ordered as MREF > CREF > BREF (see Figure 8). This is because the utilization of filler materials with larger particles forms a thicker conductive network, leading to a decrease in the scattering of interfacial phonons between filler and polymer matrix and higher TCC of polymer composites.[98] However, the incorporation of larger sizes may also cause problems such as difficulty in fabrication and inferior mechanical properties,[99] which can be countered by minimizing the scattering of phonons at the interface either via improving the interface or dispersion by filler surface treatment.[98]

The incorporation of 0.01%–0.05% SWCNTs in specimens containing filler materials increases TCC, particularly in the specimens containing barite and magnetite. For example, BSC-1 and BSC-2 increased TCC by 31.75% and 38.09% as compared to BREF, respectively. Similarly, MSC-1 and MSC-2 increased TCC by 5.88% and 3.52% as compared to MREF, respectively. The improvement of TCC in the SWCNT-reinforced specimens containing barite and magnetite can be attributed to further enhancement of interaction between the filler materials and polymer matrix, leading to the development of a more conductive network. On the other hand, the incorporation of SWCNTs in specimens containing colemanite caused no influence on the TCC. It is important to note that the TCC of specimens achieved in this study (even without implementing any special dispersion technique) is either equal to or more than previous studies with different polymer composites containing nano/micro fillers.[92,94,95,100]

3.4 | γ-Radiation shielding

Table 4 shows the density, LAC, MAC, HVL, and TVL of specimens with different filler materials and the amount of SWCNTs. As per the Table, the addition of SWCNTs decreases the density of most specimens. For example, the density of SC-1, SC-2, and SC-3 are 9.61%, 6.21%, and 2.25% lower as compared to REF, respectively, which can be attributed to the lower density of SWCNT (~0.07 g/cm^3). However, the incorporation of filler materials increased the density of specimens owing to the greater density of filler materials as compared to polymer resin. For instance, BREF, MREF, and CREF have 25.43%, 34.46%, and 6.21% higher density as compared to REF, respectively. The addition of SWCNTs decreases the density of specimens containing filler materials is similar to the specimens without filler materials. However, 0.1% and 0.05% incorporation of barite and colemanite increases the density of respective reference specimens.

TABLE 4 Density of specimens and their LAC, MAC, HVL, and TVL

Specimen	Density (g/cm^3)	Linear attenuation coefficient (μ cm^{-1})	Mass attenuation coefficient (μ_m cm^2/g)	HVL (cm)	TVL (cm)
REF	1.77	0.061	0.034	11.37	37.18
SC-1	1.6	0.04	0.025	17.38	57.74
SC-2	1.66	0.047	0.028	14.64	48.63
SC-3	1.73	0.057	0.032	12.05	40.05
BREF	2.22	0.079	0.035	8.749	29.064
BSC-1	2.21	0.059	0.026	11.725	38.949
BSC-2	2.17	0.079	0.036	8.824	29.312
BSC-3	2.29	0.101	0.044	6.871	22.825
MREF	2.38	0.084	0.035	8.239	27.369
MSC-1	2.34	0.084	0.035	8.244	27.387
MSC-2	2.36	0.085	0.036	8.131	27.011
MSC-3	2.17	0.083	0.038	8.351	27.740
CREF	1.88	0.069	0.036	9.983	33.162
CSC-1	1.88	0.069	0.036	10.051	33.388
CSC-2	1.89	0.070	0.037	9.915	32.936

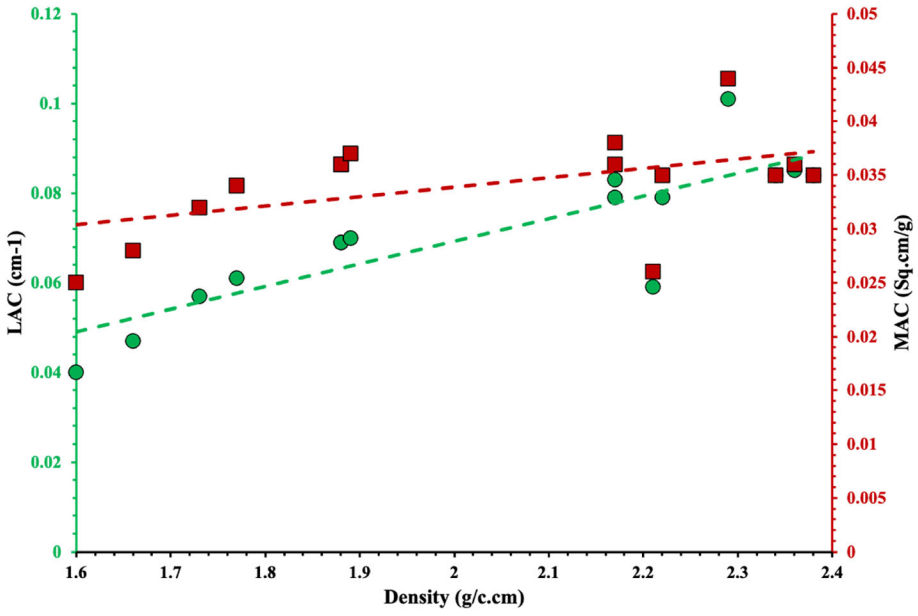

FIGURE 9 Density versus LAC/MAC of specimens with different filler materials and amount of SWCNTs [Color figure can be viewed at wileyonlinelibrary.com]

Based on the data listed in Table 4, Figure 9 shows the LAC and MAC vs density of the specimens. As per the figure, a direct relationship exists between density and LAC/MAC, which aligns with previous studies.[101,102] Figure 9 shows that SC-1 has the lowest LAC and MAC, while BSC-3 has the highest LAC and MAC. The vulnerability of neat polymer to irradiation can be attributed to the generation of free radicals in the polymer matrix, which leads to the degradation of the crosslinking network and microstructure, allowing γ-rays to penetrate.[103] The addition of SWCNTs in the polymer leads to lower LAC and MAC due to a reduction in the density of specimens. It is interesting to note that a few fluctuations can also be observed between the density and LAC/MAC, for example, though the density of MREF is greater than BSC-3, the LAC and MAC of BSC-3 are greater than MREF. This is because the higher weight/density (see Table 4) of magnetite restricts its movement and creates agglomerates and voids (see Figure 11), which aids penetration of γ-rays. Moreover, these fluctuations can also be attributed to limitations owing to the accuracy of apparatuses and other sources of uncertainties like

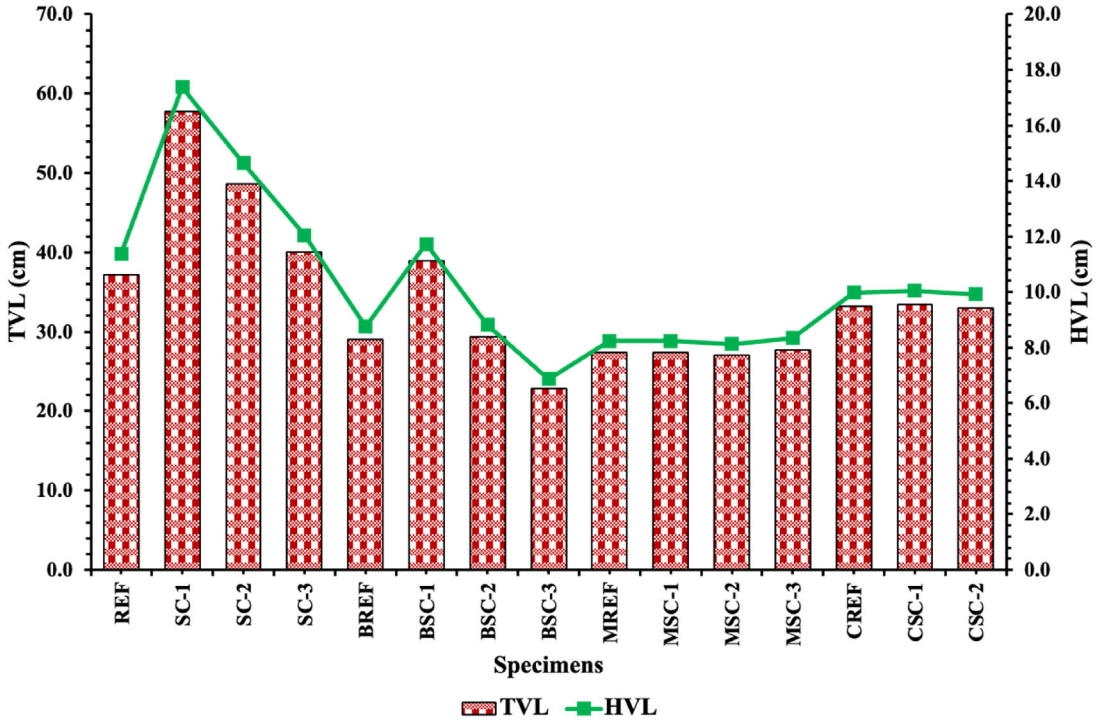

FIGURE 10 HVL and TVL of specimens with different filler materials and amount of SWCNTs [Color figure can be viewed at wileyonlinelibrary.com]

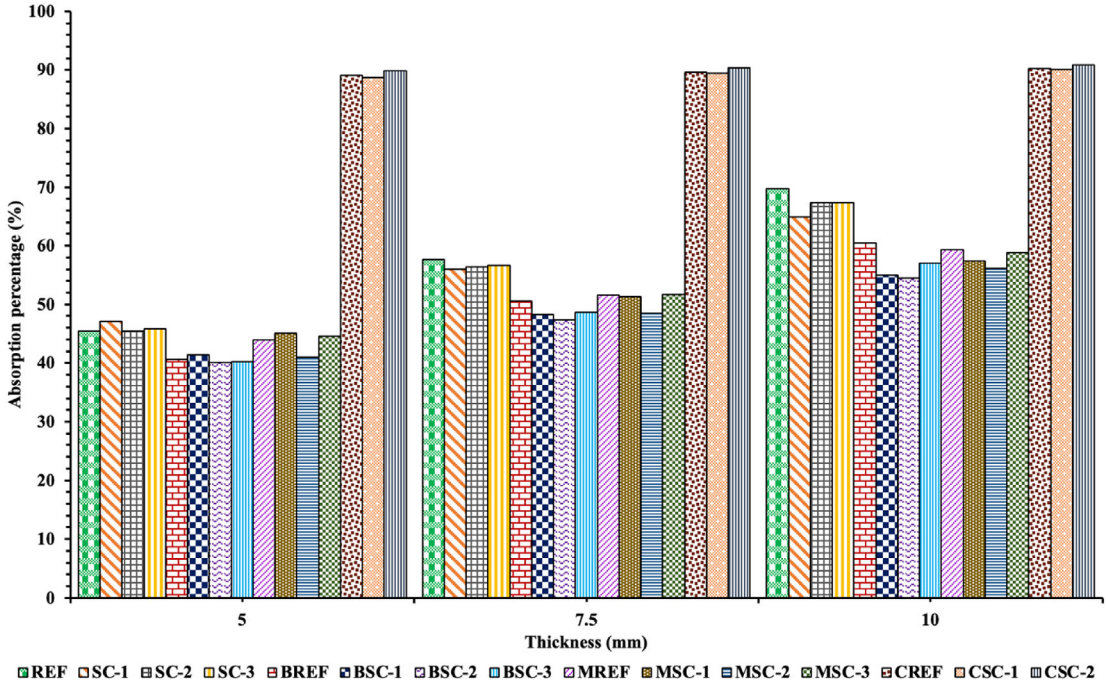

FIGURE 11 Percentage absorption of N-rays of specimens with different thickness, filler materials, and amount of SWCNTs [Color figure can be viewed at wileyonlinelibrary.com]

inhomogeneities of the specimens at various points, which is consistent with previously published experimental works.[104,105] It can be observed from Table 4 that the addition of SWCNTs significantly affects the LAC and MAC of specimens containing barite and magnetite. For instance, the LAC of BSC-1 and BSC-2 is 0.45% and 2.25% lower than that of BREF, respectively; however, BSC-3 superseded the LAC of BREF by 3.15%. A similar trend

TABLE 5 Percentage absorption of N-rays of specimens with different thickness, filler materials, and amount of SWCNTs

Specimen	Thickness (mm)	N-absorption (%)
REF	3.7	36.97
	6.95	59.01
	10.5	70.29
SC-1	4.15	42.01
	8.25	62.94
	12.4	71.39
SC-2	4.1	40.43
	7.65	59.18
	11.45	72.59
SC-3	3.7	38.58
	7.6	60.65
	11.3	71.11
BREF	4.65	36.82
	8.8	60.34
	13.5	72.31
BSC-1	5.9	43.3
	11.95	61.54
	17.8	75.76
BSC-2	5.5	39.37
	10.9	61.35
	16.6	71.31
BSC-3	4.6	37.10
	9.3	58.06
	14.9	72.03
MREF	5.25	43.78
	10.5	62.68
	15.9	76.3
MSC-1	6.3	47.09
	12.5	66.06
	18.9	78.40
MSC-2	5.55	41.68
	11.6	62.98
	16.85	75.69
MSC-3	5.35	43.41
	10.6	64.66
	16.5	75.45
CREF	7.7	89.23
	15.9	92.7
	23.7	93.11
CSC-1	8.9	90.43
	17.1	93.07
	25.45	94.07
CSC-2	8.6	89.36
	17.6	92.72
	26.8	94.09

was observed for the MAC of SWCNT-reinforced specimens containing barite. The positive impact of SWCNTs on the attenuation of γ-radiation of barite-filled specimens can be credited to the scavenging of free radicals via SWCNTs produced during irradiation.[106] On the other hand, in the case of magnetite-filled specimens, the addition of SWCNTs could not surpass the LAC/MAC of REF. Furthermore, the incorporation of SWCNTs did not impact the LAC and MAC of specimens containing colemanite.

Table 4 shows that HVL and TVL values are inversely proportional to LAC, that is, the lowest HVL and TVL values correspond to the highest LAC, which can be regarded as another considerable pattern for the excellent attenuation performance of respective specimens. HVL and TVL values of specimens listed in Table 4 are graphically presented in Figure 10. As per the figure, the determination of HVL and TVL values is supported by the thickness of specimens required to stop 50% and 90% of the incoming γ-rays. The incorporation of filler materials led to a significant decrease in the TVL and HVL values as compared to neat polymer and specimens only containing SWCNTs, indicating their better performance against incoming γ-rays. When compared to neat polymer and specimens only containing SWCNTs, the incorporation of filler materials resulted in a significant decrease in TVL and HVL values, indicating their superior performance against incoming γ -rays. By comparing the HVL/TVL values of specimens containing different filler materials, it can be observed that barite-filled specimens, due to their minimum HVL/TVL values, exhibited better performance in terms of γ-radiation shielding attenuation. Furthermore, the addition of SWCNTs in barite-filled specimens further reduced TVL and HVL values, which is not the case for SWCNT-reinforced specimens containing magnetite and colemanite.

3.5 | N-radiation shielding

Table 5 shows the N-absorption of specimens of different thicknesses, filler materials, and amount of SWCNTs. As per the Table, for a given type of filler material and amount of SWCNTs, N-rays absorption increased by increasing the thickness of the specimen because it is difficult for the N-rays to penetrate through the specimens with greater

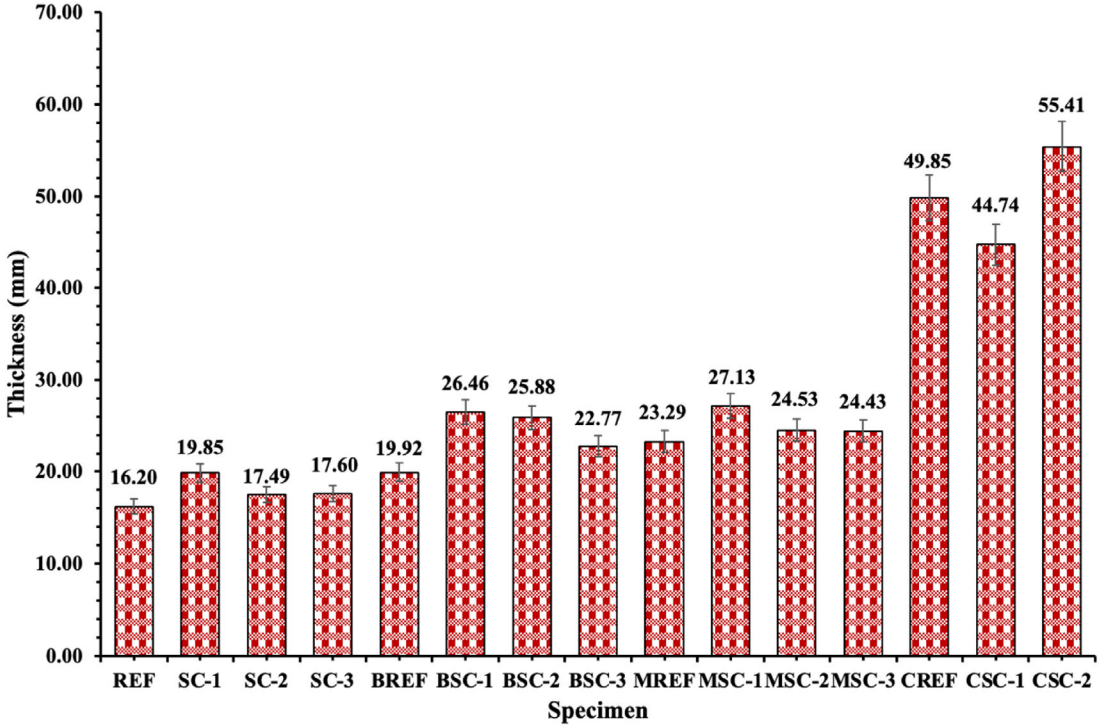

FIGURE 12 Thickness of the specimens required to absorb 100% of N-radiation [Color figure can be viewed at wileyonlinelibrary.com]

thickness. It is important to note that some specimens having greater thickness still possess lower N-absorption, which can be attributed to the presence of voids aiding the penetration of N-rays. The neat polymer (REF) has the lowest N-absorption as compared to other specimens with or without SWCNTs and filler materials. However, the addition of SWCNTs exhibited higher N-absorption as compared to the REF owing to the increase in the thickness of the specimen. Based on the N-absorption, the specimens only containing SWCNTs can be ordered as SC-1 > SC-2 > SC-3. The direct relationship between N-radiation absorption and the thickness of the specimen is consistent with the previous studies on polyethylene/boron composites,[107] nanoengineered polymer composites,[108] and polyimide/boron carbide composites.[109]

In the case of specimens containing filler materials, N-absorption further increased owing to the increase in the thickness of the specimen. By comparing the N-absorption of filler-modified specimens, colemanite-containing specimens superseded the N-absorption of barite and magnetite-filled specimens. Based on the N-absorption efficiency, specimens containing filler materials can be ordered as CREF > MREF > BREF. However, the addition of SWCNTs poses a variable impact on the N-absorption of filler material added specimens. For instance, based on the N-absorption efficiency, SWCNT-reinforced specimens containing colemanite and magnetite can be ordered as CSC1 > CSC-2 and MSC-1 > MSC-2 > MSC-3, respectively. On the other hand, based on the N-absorption efficiency, SWCNT-reinforced specimens containing barite can be ordered as BSC-1 > BSC-2 > BSC-3.

To better estimate the N-absorption efficiency of specimens, the data listed in Table 5 was used to calculate the N-absorption of specimens with a constant thickness of 5, 7.5, and 10 mm. Figure 11 shows the percentage absorption of specimens with different thicknesses, filler materials, and amount of SWCNTs. As per the figure, for a given type of filler material and amount of SWCNTs, N-rays absorption increased by increasing the thickness of the specimen. At different thicknesses, The N-absorption of neat polymer (REF) is higher in most specimens only containing SWCNTs (SC-1, SC-2, and SC-3). In addition, barite- and magnetite-filled specimens with 5, 7.5, and 10 mm reduced the N-absorption, which may be attributed to poor interfacial adhesion between polymer resin and filler materials (barite and magnetite). For example, 5, 7.5, and 10 mm thick BREF specimens exhibited 10.54%, 12.19%, and 13.28% as compared to REF with similar thickness. MREF, like BREF, experienced a decreasing trend in N-absorption; however, MREF's N-absorption was greater than BREF's. The colemanite-filled specimens with or without SWCNTs considerably superseded the N-absorption as compared to other specimens prepared, which can be ascribed to strong interfacial adhesion between colemanite and polymer resin. The N-radiation results obtained for this study are consistent with previous studies in which N-radiation shielding

for poly(methyl methacrylate) composites containing 10%–40% colemanite was evaluated.[110]

Based on the data listed in Table 5, the average thickness for specimens to absorb 100% of N-rays was calculated and graphically illustrated in Figure 12. As per the figure, to ensure 100% absorption of N-radiation, REF and CSC-2 require the minimum and maximum thickness, respectively. The specimen thickness requirement for specimens containing only SWCNTs is slightly increased as compared to REF. Comparing the required thickness of the specimens containing barite and magnetite, thickness required for barite-filled specimens (with or without SWCNTs) is slightly greater than magnetite-filled specimens. Similar to the substantial increase in the N-absorption of colemanite-filled specimens (see Figure 11), the required thickness of 100% N-absorption of colemanite-filled specimens is also greater as compared to other specimens.

4 | CONCLUSIONS

In this study, mechanical and radiation shielding properties of polyester/GF-based composites containing different filler materials and amount of SWCNTs were investigated. The specimens were evaluated against tensile strength, flexural strength, Charpy impact strength, γ-radiation shielding, and N-radiation shielding. Based on the results and discussion, the following conclusions can be deduced:

1. The incorporation of SWCNTs and filler materials increases the viscosity of polymer resin. This can be credited to the strong van der Waals forces between SWCNTs and the high density/weight of filler materials leading to agglomeration. Colemanite-filled specimens experienced a substantial increase in viscosity (12,200 mPa.s) due to the transition from a liquid state to a solid state, making it difficult to cast specimens containing colemanite and evaluate their mechanical properties.
2. The addition of SWCNTs is beneficial to increase the tensile strength and flexural strength of the specimens because of the strong interfacial adhesion between SWCNTs and polymer resin, which prevents the growth of cracks. However, the incorporation of barite and magnetite reduced the tensile strength and flexural strength by approximately 50% as compared to REF and SWCNT-reinforced specimens. Nonetheless, barite-filled specimens experienced higher tensile strength and flexural strength as compared to magnetite-filled specimens.
3. Unlike tensile/flexural strength, the impact strength of specimens containing filler materials performed well, that is, most of the barite and magnetite-added specimens exhibited slightly lower impact strength than the neat polymer and SWCNT-added specimens. In addition, BREF experienced 32.56%, 65.22%, 43.4%, and 9.43% higher impact strength as compared to REF, SC-1, SC-2, and SC-3, respectively.
4. In the case of TCC, specimens containing both filler materials and SWCNTs performed exceptionally well. Specimens like BSC-1, BSC-2, MREF, MSC-1, MSC-2, CREF, CSC-1, and CSC-3 showed 30.56%–60% higher TCC as compared to REF and SWCNT reinforced specimens. This is because filler materials and SWCNTs aid in the formation of conduction paths throughout the specimens, making them suitable for radiation shielding applications where the accumulation of heat is a critical problem.
5. The specimens containing only barite and magnetite exhibited the highest LAC and MAC due to the increase in the density of the specimen. In addition, SWCNT-reinforced specimens (such as BSC-3, MSC-2, and MSC-3) also exhibited better results for LAC and MAC, which can be ascribed to the scavenging of free radicals via SWCNTs produced during irradiation.
6. The N-absorption of specimens containing filler materials is higher than the neat polymer and specimens containing SWCNTs owing to the greater thickness. By keeping the thickness constant at 5, 7.5, and 10 mm, the difference in N-absorption of specimens with and without filler materials (except colemanite) is not significant. Either with constant or variable thickness of specimens, colemanite-filled specimens outperformed other specimens in absorbing N-rays, which can be attributed to strong interfacial adhesion between colemanite and polymer resin.

The findings of this study are encouraging, revealing that it is possible to develop SWCNT-reinforced polyester/GF-based composite plates with adequate mechanical strength and excellent radiation shielding properties using readily available filler materials.

AUTHOR CONTRIBUTIONS

Ali Murat Sürücü: Conceptualization (lead); data curation (lead); formal analysis (lead); investigation (lead); methodology (lead); validation (lead); writing – review and editing (lead). **Serkan Subaşı:** Conceptualization (lead); data curation (lead); formal analysis (lead); validation (lead); writing – review and editing (lead). **Aamar Danish:** Formal analysis (lead); investigation (lead); methodology (lead); writing – original draft (lead); writing – review and editing (lead). **Osman Gencel:** Conceptualization (supporting); data curation (supporting); formal analysis (supporting); methodology (supporting); supervision (lead); writing – review and

editing (supporting). **Azime Subaşı:** Formal analysis (supporting); methodology (supporting); validation (supporting); writing – review and editing (supporting). **Togay Ozbakkaloglu:** Conceptualization (equal); methodology (lead); supervision (lead); validation (lead); writing – review and editing (lead).

FUNDING INFORMATION

No funding was acquired for this research.

CONFLICT OF INTEREST

All authors declare no conflicts of interest.

DATA AVAILABILITY STATEMENT

The data that support the findings of this study are available on request from the corresponding author.

ORCID

Aamar Danish https://orcid.org/0000-0002-2905-3638
Togay Ozbakkaloglu https://orcid.org/0000-0003-3015-736X

REFERENCES

[1] A. Abdelnour-Esquivel, J. Perez, M. Rojas, W. Vargas, A. Gatica-Arias, *In Vitro Cell Dev Biol Plant* **2020**, *56*, 88.
[2] M. Parasuraman, P. Weerasinghe, *Mutation Breeding, Genetic Diversity and Crop Adaptation to Climate Change*, CAB International, Glasgow **2021**, pp. 76–82. https://doi.org/10.1079/9781789249095.0008
[3] S. Shahi, R. Khorvash, M. Goli, S. M. Ranjbaran, A. Najarian, A. Mohammadi Nafchi, *Food Sci Nutr* **2021**, *9*, 5883.
[4] S. Nair, M. Engelbrecht, X. Miles, R. Ndimba, R. Fisher, P. du Plessis, J. Bolcaen, J. Nieto-Camero, E. de Kock, C. Vandevoorde, *Int. J. Mol. Sci.* **2019**, *20*, 5350.
[5] H. Tekin, E. Altunsoy, E. Kavaz, M. Sayyed, O. Agar, M. Kamislioglu, *Results Phys* **2019**, *12*, 1457.
[6] H. Albander, M. I. Aljalis, New trends in preparation, bio distribution, and pharmacokinetics of radiopharmaceuticals in diagnosis and research, **2022**.
[7] T. C. Weekes, *Very High Energy Gamma-Ray Astronomy*, CRC Press, Boca Raton **2003**.
[8] M. Ajello, M. Di Mauro, V. Paliya, S. Garrappa, *Astrophys J* **2020**, *894*, 88.
[9] M. Litvak, Y. N. Barmakov, S. G. Belichenko, E. P. Bogolubov, A. S. Kozyrev, I. G. Mitrofanov, A. V. Nosov, A. S. Perkhov, A. V. Samoshin, A. B. Sanin, S. E. Sholeninov, V. N. Shvetsov, D. I. Yurkov, A. O. Zontikov, V. I. Zverevb, *Nuclear Instrum Methods Phys Res A Accelerators Spectrometers Detectors Associated Equipment* **2020**, *963*, 163725.
[10] C. V. More, Z. Alsayed, M. Badawi, A. Thabet, P. P. Pawar, *Environ. Chem. Lett.* **2021**, *19*, 2057.
[11] C. E. Okafor, U. C. Okonkwo, I. P. Okokpujie, *J. Mater. Sci.* **2021**, *56*, 11631.
[12] S. Nambiar, J. T. Yeow, *ACS Appl. Mater. Interfaces* **2012**, *4*, 5717.
[13] N. J. AbuAlRoos, M. N. Azman, N. A. B. Amin, R. Zainon, *Phys Med* **2020**, *78*, 48.
[14] P. R. D'Auria Vieira de Godoy, A. Nakamura, A. P. Khavari, T. Sangsuwan, S. Haghdoost, *Environ. Mol. Mutagen.* **2021**, *62*, 422.
[15] R. Adeli, S. P. Shirmardi, S. J. Ahmadi, *Radiat. Phys. Chem.* **2016**, *127*, 140.
[16] J. Guo, P. Gougeon, X.-G. Chen, *Compos B* **2012**, *43*, 2400.
[17] Y. Huang, W. Zhang, L. Liang, J. Xu, Z. Chen, *Chem. Eng. J.* **2013**, *220*, 143.
[18] S. A. Issa, A. Mostafa, T. A. Hanafy, M. Dong, X. Xue, *Prog. Nucl. Energy* **2019**, *111*, 15.
[19] G. A. Eid, A. Kany, M. El-Toony, I. Bashter, F. Gaber, *Arab. J. Nucl. Sci. Appl* **2013**, *46*, 226.
[20] S. Joshi, V. Snehalatha, K. Sivasubramanian, D. Ponraju, V. Jayaraman, B. Venkatraman, *J. Mater. Eng. Perform.* **2019**, *28*, 7332.
[21] N. Abdelal, R. Abu Saleem, A. Alsabbagh, M. Al-Jarrah, F. Al-Jawarneh, *J. Compos. Mater.* **2022**, *56*, 00219983221101989.
[22] R. Li, Y. Gu, Y. Wang, Z. Yang, M. Li, Z. Zhang, *Mater Res Exp* **2017**, *4*, 035035.
[23] K. Verdipoor, A. Alemi, A. Mesbahi, *Radiat. Phys. Chem.* **2018**, *147*, 85.
[24] L. Chang, Y. Zhang, Y. Liu, J. Fang, W. Luan, X. Yang, W. Zhang, *Nuclear Instrum Methods Phys Res B Beam Interactions Mater Atoms* **2015**, *356*, 88.
[25] H. Hassan, H. Badran, A. Aydarous, T. Sharshar, *Nuclear Instrum Methods Phys Res B Beam Interactions Mater Atoms* **2015**, *360*, 81.
[26] R. Rajavikraman, P. Nitin, *Int J Mater Sci Eng* **2013**, *1*, 20.
[27] A. A. El-Sayed, I. N. Fathy, B. A. Tayeh, I. Almeshal, *Constr. Build. Mater.* **2022**, *324*, 126663.
[28] N. Jauhari, R. Mishra, H. Thakur, *Mater Today Proc* **2015**, *2*, 2868.
[29] A. Warrier, A. Godara, O. Rochez, L. Mezzo, F. Luizi, L. Gorbatikh, S. V. Lomov, A. W. VanVuure, I. Verpoest, *Compos A Appl Sci Manuf* **2010**, *41*, 532.
[30] T. Sathishkumar, S. Satheeshkumar, J. Naveen, *J. Reinf. Plast. Compos.* **2014**, *33*, 1258.
[31] W.-M. Qian, M. H. Vahid, Y. L. Sun, A. Heidari, R. Barbaz-Isfahani, S. Saber-Samandari, A. Khandan, D. Toghraie, *J Mater Res Technol* **2021**, *12*, 1931.
[32] V. Harish, N. Nagaiah, T. N. Prabhu, K. Varughese, *J. Appl. Polym. Sci.* **2009**, *112*, 1503.
[33] Q. Li, Q. Wei, W. Zheng, Y. Zheng, N. Okosi, Z. Wang, M. Su, *ACS Appl. Mater. Interfaces* **2018**, *10*, 35510.
[34] F. Özkalaycı, M. R. Kaçal, O. Agar, H. Polat, A. Sharma, F. Akman, *J. Phys. Chem. Solids* **2020**, *145*, 109543.
[35] A. Erol, I. Pocan, E. Yanbay, O. A. Ersoz, F. Y. Lambrecht, *Radiat Protection Environ* **2016**, *39*, 3.
[36] A. K. Singh, R. K. Singh, B. Sharma, A. K. Tyagi, *Radiat. Phys. Chem.* **2017**, *138*, 9.
[37] R. A. Abu Saleem, N. Abdelal, A. Alsabbagh, M. Al-Jarrah, F. Al-Jawarneh, *Polymer* **2021**, *13*, 3699.
[38] N. Nagaraja, H. Manjunatha, L. Seenappa, K. Sridhar, H. Ramalingam, *Radiat. Phys. Chem.* **2020**, *171*, 108723.
[39] A. Hashim, A. Hadi, *Ukr. J. Phys.* **2017**, *62*, 978.
[40] F. Akman, H. Ogul, I. Ozkan, M. R. Kaçal, O. Agar, H. Polat, K. Dilsiz, *Nuclear Eng Technol* **2022**, *54*, 283.
[41] F. Akman, H. Ogul, M. Kaçal, H. Polat, K. Dilsiz, M. Turhan, *Appl Phys A* **2020**, *126*, 1.
[42] G. Rabilloud, *Handbook of Adhesives and Sealants*, Vol. 1, Elsevier, Amsterdam, Netherlands **2005**, p. 349.

[43] C. May, *Epoxy Resins: Chemistry and Technology*, Routledge, Basel **2018**.
[44] S. Wang, Z. Liang, B. Wang, C. Zhang, *Adv. Mater.* **2007**, *19*, 1257.
[45] S. Wang, *Curr Appl Phys* **2009**, *50*, 1146.
[46] S. Wang, *J. Mater. Sci.* **2008**, *43*, 5837.
[47] M. H. Al-Saleh, U. Sundararaj, *Carbon* **2009**, *47*, 1738.
[48] A. I. Ebunu, Y. A. Olanrewaju, O. Ogolo, A. R. Adetunji, A. P. Onwualu, *Heliyon* **2021**, *7*, e07365.
[49] M. Gonen, E. Nyankson, R. B. Gupta, *Ind. Eng. Chem. Res.* **2016**, *55*, 5116.
[50] T. Uysal, H. S. Mutlu, M. Erdemoğlu, *Int. J. Miner. Process.* **2016**, *151*, 51.
[51] K. Okuno, *Radiat. Prot. Dosim.* **2005**, *115*, 258.
[52] T. Korkut, A. Ün, F. Demir, A. Karabulut, G. Budak, R. Şahin, M. Oltulu, *Ann. Nucl. Energy* **2010**, *37*, 996.
[53] E. I. Anastasova, D. Puzyrev, V. Ivanovski, A. S. Drozdov, *J. Magn. Magn. Mater.* **2020**, *503*, 166619.
[54] J. Roger, J. Pons, R. Massart, A. Halbreich, J. Bacri, *Eur Phys J Appl Phys* **1999**, *5*, 321.
[55] A. Jordan, R. Scholz, P. Wust, H. Fähling, R. Felix, *J. Magn. Magn. Mater.* **1999**, *201*, 413.
[56] B. Oto, A. Gür, E. Kavaz, T. Çakır, N. Yaltay, *Prog. Nucl. Energy* **2016**, *92*, 71.
[57] A. O. G. Posada, D. A. L. Téllez, J. Roa-Rojas, J. R. R. Barrado, *J Mater Res Technol* **2020**, *9*, 10597.
[58] S. Oswald, W. Kinzelbach, A. Greiner, G. Brix, *Geoderma* **1997**, *80*, 417.
[59] ISO 2535, *Plastics-Unsaturated-Polyester Resins-Measurement of Gel Time at Ambient Temperature*, ISO, Tokyo, Japan **2001**.
[60] I. ISO 2555, *Plastics-Resins in the Liquid State or as Emulsions or Dispersions—Determination of Apparent Viscosity by the Brookfield Test Method*, International Organization of Standards, Geneva, Switzerland **2018**.
[61] ISO 527-4, *Plastics—Determination of Tensile Properties—Part 4: Test Conditions for Isotropic and Orthotropic Fibre-Reinforced Plastic Composites*, I. O. f. Standardization, Tokyo, Japan **2021**.
[62] ASTM D7264/D7264M-07, *Standard Test Method for Flexural Properties of Polymer Matrix Composite Materials*, ASTM International, West Conshohocken **2007**. https://doi.org/10.1520/D7264_D7264M-07
[63] ISO 179-2, *Plastics—Determination of Charpy Impact Properties—Part 2: Instrumented Impact Test*, I. O. f. Standardization, Beijing **2020**.
[64] J. Zhu, C. Abeykoon, N. Karim, *Int J Lightweight Mater Manuf* **2021**, *4*, 370.
[65] A. Patti, D. Acierno, H. Lecocq, A. Serghei, P. Cassagnau, *Rheol. Acta* **2021**, *60*, 661.
[66] Z. Li, G. Luo, F. Wei, Y. Huang, *Compos Sci Technol* **2006**, *66*, 1022.
[67] L. Lozano-Sánchez, A. O. Sustaita, M. Soto, S. Biradar, L. Ge, E. Segura-Cárdenas, J. Diabb, L. E. Elizalde, E. V. Barrera, A. Elías-Zúñiga, *J. Mater. Process. Technol.* **2017**, *242*, 218.
[68] I. Otero-Navas, M. Arjmand, U. Sundararaj, *Polymer* **2017**, *114*, 122.
[69] L. Lavagna, R. Nisticò, S. Musso, M. Pavese, *Mater Today Chem* **2021**, *20*, 100477.
[70] F. Zaccardi, M. G. Santonicola, S. Laurenzi, *Compos Struct* **2021**, *255*, 113050.
[71] X. Liu, C. Li, Y. Pan, D. W. Schubert, C. Liu, *Compos B* **2019**, *164*, 37.
[72] J. Jyoti, S. Dhakate, B. P. Singh, *Compos B* **2018**, *154*, 337.
[73] S. A. Madkour, S. Tirkes, U. Tayfun, *Appl Surf Sci Adv* **2021**, *3*, 100042.
[74] M. Ayatollahi, R. Barbaz Isfahani, R. Moghimi Monfared, *J. Compos. Mater.* **2017**, *51*, 4177.
[75] D. Banerjee, T. Nguyen, T.-J. Chuang, *Comput. Mater. Sci.* **2016**, *114*, 209.
[76] M. L. Manchado, L. Valentini, J. Biagiotti, J. Kenny, *Carbon* **2005**, *43*, 1499.
[77] X. Li, H. Gao, W. A. Scrivens, D. Fei, X. Xu, M. A. Sutton, A. P. Reynolds, M. L. Myrick, *J. Nanosci. Nanotechnol.* **2007**, *7*, 2309.
[78] B. Hornbostel, P. Pötschke, J. Kotz, S. Roth, *Phys. Status Solidi B* **2006**, *243*, 3445.
[79] G. Guzel, O. Sivrikaya, H. Deveci, *Compos B* **2016**, *100*, 1.
[80] H. Y. Kordkheili, S. Hiziroglu, M. Farsi, *Mater. Des.* **2012**, *33*, 395.
[81] X. Shi, J. L. Hudson, P. P. Spicer, J. M. Tour, R. Krishnamoorti, A. G. Mikos, *Nanotechnol* **2005**, *16*, S531.
[82] H. Y. Kordkheili, M. Farsi, Z. Rezazadeh, *Compos B* **2013**, *44*, 750.
[83] K. Y. Cho, H. Park, H. J. Kim, X. H. do, C. M. Koo, S. S. Hwang, H. G. Yoon, K. Y. Baek, *Compos Sci Technol* **2018**, *157*, 21.
[84] S. Li, Y. Yao, *Compos B* **2019**, *165*, 293.
[85] J. Makar, J. Margeson, and J. Luh, "Carbon nanotube/cement composites-early results and potential applications," in Proc Third Int Conf Const Mater Perform Innov Struct Implic, Vancouver Canada, **2005**, pp. 1–10.
[86] S. Hulsey, S. Absar, Q. N. Sultana, S. M. Sabet, H. Mahfuz, M. Khan, *Polym. Compos.* **2018**, *39*, E1025.
[87] M. El-Sarraf, A. E.-S. Abdo, *Radiat. Phys. Chem.* **2013**, *88*, 21.
[88] A. C. Roulin-Moloney, *Fractography and Failure Mechanisms of Polymers and Composites*, Springer, Essex **1989**.
[89] R. Huang, X. Zhang, C. Zhou, *Wood Sci. Technol.* **2020**, *54*, 1299.
[90] Y. Xu, X. Wang, J. Zhou, B. Song, Z. Jiang, E. M. Y. Lee, S. Huberman, K. K. Gleason, G. Chen, *Sci. Adv.* **2018**, *4*, eaar3031.
[91] S. Yang, W. Li, S. Bai, Q. Wang, *ACS Appl. Mater. Interfaces* **2018**, *11*, 3388.
[92] S. Y. Pak, H. M. Kim, S. Y. Kim, J. R. Youn, *Carbon* **2012**, *50*, 4830.
[93] S. T. Huxtable, D. G. Cahill, S. Shenogin, L. Xue, R. Ozisik, P. Barone, M. Usrey, M. S. Strano, G. Siddons, M. Shim, P. Keblinski, *Nat. Mater.* **2003**, *2*, 731.
[94] S. Wang, R. Liang, B. Wang, C. Zhang, *Carbon* **2009**, *47*, 53.
[95] E. M. Jackson, P. E. Laibinis, W. E. Collins, A. Ueda, C. D. Wingard, B. Penn, *Compos B* **2016**, *89*, 362.
[96] Y. Xu, G. Ray, B. Abdel-Magid, *Compos A Appl Sci Manuf* **2006**, *37*, 114.
[97] G.-W. Lee, J. I. Lee, L. Sang-Soo, M. Park, J. Kim, *J. Mater. Sci.* **2005**, *40*, 1259.
[98] G.-W. Lee, M. Park, J. Kim, J. I. Lee, H. G. Yoon, *Compos A Appl Sci Manuf* **2006**, *37*, 727.
[99] X. Huang, P. Jiang, T. Tanaka, *IEEE Electr Insul Mag* **2011**, *27*, 8.
[100] J. Zhang, S. Qi, *Polym. Compos.* **2014**, *35*, 381.

[101] K. Bagheri, S. M. Razavi, S. J. Ahmadi, M. Kosari, H. Abolghasemi, *Radiat. Phys. Chem.* **2018**, *146*, 5.
[102] M. E. Mahmoud, A. M. El-Khatib, M. S. Badawi, A. R. Rashad, R. M. El-Sharkawy, A. A. Thabet, *Radiat. Phys. Chem.* **2018**, *145*, 160.
[103] M. Marrale, A. Longo, S. Panzeca, S. Gallo, F. Principato, E. Tomarchio, A. Parlato, A. Buttafava, D. Dondi, A. Zeffiro, *Nuclear Instrum Methods Phys Res B Beam Interactions Mater Atoms* **2014**, *339*, 15.
[104] R. Mehrara, S. Malekie, S. M. S. Kotahi, S. Kashian, *Sci. Rep.* **2021**, *11*, 1.
[105] N. Rostampour, T. Almasi, M. Rostampour, M. Mohammadi, K. Ghazikhanlou Sani, H. R. Khosravi, S. M. H. Pooya, B. Golzar, N. Jabari Vesal, *Radiat. Prot. Dosim.* **2012**, *152*, 438.
[106] X. Shi, B. Jiang, J. Wang, Y. Yang, *Carbon* **2012**, *50*, 1005.
[107] C. Harrison, E. Burgett, N. Hertel, and E. Grulke, "," in *AIP Conference Proceedings*, vol. 969, American Institute of Physics, Albuquerque **2008**, pp. 484–491.
[108] N. A. Galehdari, A. D. Kelkar, *J. Mater. Res.* **2017**, *32*, 426.
[109] X. Li, J. Wu, C. Tang, Z. He, P. Yuan, Y. Sun, W. M. Lau, K. Zhang, J. Mei, Y. Huang, *Compos B* **2019**, *159*, 355.
[110] T. Bel, C. Arslan, N. Baydogan, *Mater. Chem. Phys.* **2019**, *221*, 58.

SUPPORTING INFORMATION

Additional supporting information can be found online in the Supporting Information section at the end of this article.

How to cite this article: A. M. Sürücü, S. Subaşı, A. Danish, O. Gencel, A. Subaşı, T. Ozbakkaloglu, *J. Appl. Polym. Sci.* **2023**, *140*(7), e53483. https://doi.org/10.1002/app.53483